High Resolution Transmission Electron Microscopy: Fables, Facts and Figures

W. Van Renterghem, M. Verwerft
SCK•CEN, Boeretang 200, 2400 Mol, Belgium

Abstract

Transmission electron microscopy (TEM) has been applied in solid state research since more than five decades. Yet, its application in nuclear materials research is rather limited. The main reason for a limited use of TEM on active material investigation relates to the obvious difficulties of sample preparation. In many aspects, however, only TEM is capable of providing answers on materials problems. Domains such as interfaces between dissimilar materials (a metal and its oxide; substrate and coating etc.) can only be visualized by TEM techniques. In this presentation, we will document two particular TEM techniques, namely High Resolution Electron Microscopy (HREM), i.e. the direct visualization of the atomic lattice, and micro- (or nano-) probe Energy Dispersive X-ray Spectroscopy (EDS) for the determination of the chemical composition of the specimen. The combination of these two techniques in a single instrument has only become possible with the recent evolution in TEM instruments. One can achieve this improvement either by using field-emission gun (FEG)-based microscopes or by using the latest condenser lens technology. The investigation of the oxide layer formed on a Zircaloy-4 cladding material will be used to present applications of interface research obtained with a microscope equipped with a conventional electron source and advanced condenser lens technology.

Introduction

Many macroscopic properties of the material are determined by their microscopic configuration. For example, carbon can crystallize as graphite having a hexagonal unit cell or diamond having a face centered cubic unit cell. Moreover, changes in the macroscopic behavior are often the result of changes in the general or local microstructure. For example in Zircaloy-4 cladding, the high energy radiation in a nuclear reactor increases the corrosion rate [1] and induces morphological changes known as irradiation growth [2,3]. On the microscopic level these phenomena are related to the formation of vacancies, interstitials and dislocation loops [4,5] and to the amorphization of second phase particles [6,7].

Furthermore, often two types of material, having a different crystal structure, are in contact with each other. The addition of Zr liner on Zircaloy-4 cladding or the formation of an oxide layer on the cladding due to corrosion, are examples of these interfaces. The coherence of the two phases and the organization of the atoms at the interface will influence the macroscopic properties and have to be investigated on a microscopic level.

The technique that is most suited to investigate the microstructure of the material is transmission electron microscopy (TEM). A short introduction to TEM will be given here, but more information can be found in [8,9,10]. The electrons accelerated by a high voltage have a much shorter wavelength than visible light and allow obtaining a much higher resolution. With this technique columns of atoms can be visualized, showing a projection of the crystal structure. The interaction of the electrons with the specimen can be used to characterize the defects. Part of the electrons is diffracted by the specimen, which means that they are scattered elastically along discrete directions determined by the symmetry of the crystal structure. The diffraction pattern can be visualized by imaging the back focal plane of the objective lens. From the diffraction pattern the symmetry of the crystal, the interplanar distances and the

crystal orientation can be determined. Figure 1a shows the diffraction pattern of Zircaloy-4 oriented along the $[11\bar{2}\bar{3}]$ zone. Each reflection is the result of the diffraction at one set of planes indicated by their Miller indices. The 000 reflection corresponds with the transmitted beam.

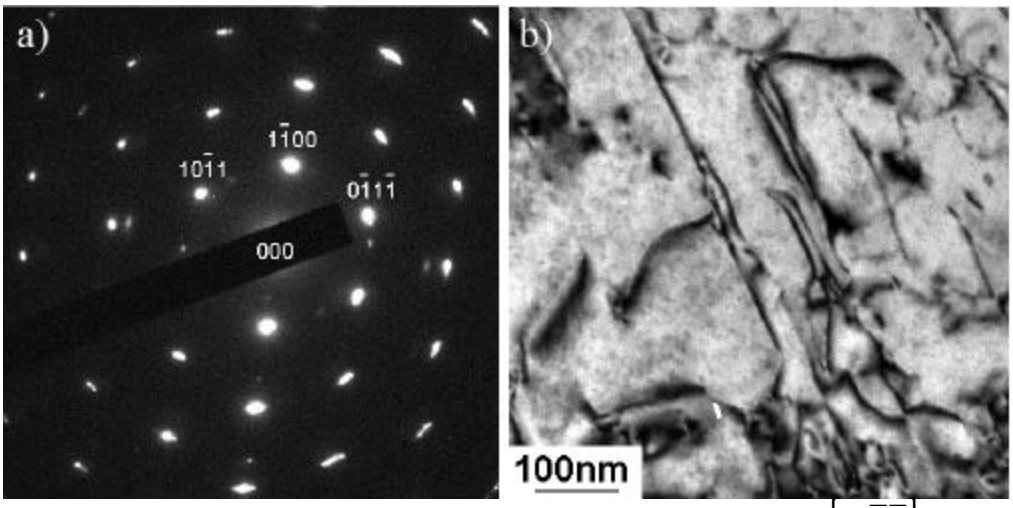

Figure 1. a) Diffraction pattern of Zircaloy-4 oriented along the $[11\bar{2}\bar{3}]$ zone. b) Conventional TEM image showing the presence of dislocations.

Projecting the image plane of the objective lens will show an enlarged image of the specimen. If by inserting an aperture only the transmitted or one diffracted beam is transmitted, the image contrast will be determined by the diffraction contrast. This kind of image is called a conventional TEM (CTEM) image. Parts of the specimen having a different orientation or crystal structure will have a different intensity. Using this contrast it is possible to localize and characterize defects. Deviations from the perfect lattice lead to local different diffraction conditions and to differences in intensity in the image. Each kind of defect introduces a specific contrast that allows the localization and characterization of the defects. Figure 1b shows for example the line contrast introduced by dislocations in Zircaloy-4. The resolution of images determined by the diffraction contrast is limited to about 1nm.

The minimal resolution required to visualize the atomic planes of simple crystal structures is 2Å. This resolution can be achieved by the interference of multiple electron beams. The contrast is no longer determined by the diffraction conditions but by the difference in phase. The resolution is limited by the quality of the lens systems and is reflected in the phase transfer function, which shows the phase shift as a function of image detail. At a certain defocus, called Sherzer defocus, the phase transfer function is constant to about 2Å. This means that a directly interpretable image of the crystal structure is obtained up to a resolution of 2Å. More detailed information is present, but does not have the correct phase. Using image simulations it is possible to retrieve this information from the image. Therefore, a second resolution is defined, called information limit, which indicates the resolution that can be obtained after image simulations.

Because the contrast is the result of the interference of different electron beams, it is possible that not all atom columns are visible. For example, light atoms will induce only a small phase shift and are often not visible in HREM images. Moreover, a shift in height of one atom column over half a unit cell might result in its extinction in the image. Therefore image simulations are always recommended for the correct interpretation of the image contrast.

From the contrast in TEM images no chemical information can be obtained about the sample. During the interaction of the electron beam with the specimen, part of the electrons is scattered inelastically thereby exciting the atoms in the specimen. The subsequent relaxation processes generate X-ray photons with an energy that is specific to the atom. From the analysis of the emitted X-rays with Energy Dispersive X-ray Spectroscopy (EDX) the composition of the specimen can be determined quantitatively. By focusing the electron beam to a very fine probe with a beam diameter up to 1nm the local composition of the specimen can be determined. The energy resolution of the technique is 0.1keV and the minimal concentration that can be detected is 0.1wt%. Apart from the signals generated by the elements of the specimen, some background signals are generally observed. There is a continuous background signal which is very low. This background mainly limits the detection limit. A copper signal is generated by the copper parts of the specimen holder and can be eliminated by using a beryllium holder. Also a carbon signal is usually present as the result of carbon deposition, introduced by the oil diffusion pumps, on the specimen. This contamination can be reduced by trapping the carbon at an anti-contamination device. Radioactive specimens might generate X-rays that correspond with the energy of a different atom. For example, X-rays generated by ^{55}Fe corresponds with the signal of Mn. Therefore a careful interpretation of the spectra is required.

TEM is a destructive technique. Because of the strong interaction between the electrons and the specimen, the thickness of the specimen must be reduced to below 200nm for conventional TEM and even to below 50nm for high resolution TEM. Moreover, it must be avoided that during specimen preparation the crystal structure changes or that extra defects are introduced. The most frequently applied techniques are mechanical polishing for the initial thinning up to a thickness of about 100µm and electrochemical polishing or ion beam milling for the final thinning steps. The specimen preparation is a crucial step which requires advanced operation tools and operator skills.

Because of the small dimensions of the TEM specimen, most manipulations have to be done by hand and can not be performed in hot cell. To reduce the activity, the specimens are cut as small as possible before further treatment. The mechanical polishing is performed in glove box. The electrochemical polishing and specimen mounting are done in a fume cupboard. This limits the maximal activity of the specimen that can be treated. Once inside the microscope there is a shielding by the microscope wall. This shielding is also required to reduce the radiation produced by the interaction between specimen and electron beam under normal operation.

For this presentation, the capabilities of TEM to investigate the microstructure of materials and interfaces will be shown. As an example, the formation of an oxide layer on Zircaloy-4 cladding formed during autoclave corrosion experiments will be presented.

The Zircaloy-4 is a passive metal. This means that the metal does not erode, but that an oxide layer is formed that slows down the corrosion of the metal. The oxidation kinetic is closely related to the grain and crystal structure of the oxide layer. It is divided in two regions: the pre- and post-transition region. The pre-transition region is marked by a cubic rate law, while the post-transition region is characterized by an accelerated oxidation and a linear rate law [11]. The different rate laws are related to differences in microstructure of the oxide layer.

At room temperature and under the conditions applied in a nuclear reactor, the monoclinic oxide phase is the thermodynamic stable phase. Above 1150°C the monoclinic phase is transformed into a tetragonal oxide phase. When a high pressure is applied, the tetragonal phase is also stabilized below the transition temperature. In literature it is reported that in the pre-transition region a dense tetragonal oxide layer is formed that acts as a barrier layer against further oxidation [11,12]. In the post-transition region, the tetragonal oxide is transformed in the monoclinic phase. The small increase in volume introduces cracks and pores in the oxide layer allowing a quicker diffusion of oxygen atoms to the metal surface and an increased oxidation rate.

Experimental

A stress-relief annealed Zircaloy-4 cladding tube has been corroded in steam at a temperature of 400°C and a pressure of 10.3MPa for 1 day in a PARR autoclave according to the ASTM standard procedure. The measured weight gain was 10.5 mg/dm². The transition under these conditions occurs after about 20 days, which means that this specimen is still in the pre-transition region.

The corroded tubes were cut into segments parallel to the tube axis. Out of these segments small bars are cut perpendicular to the tube axis. Two of these bars are glued one on top of the other. Next the specimen is mechanically polished to a thickness of about 30µm using SiC abrasive paper. The final thinning is done with ion beam milling until the area of the interface between the oxide layer and the metal is thin enough.

The specimens have been investigated in a JEOL 3010 TEM operating at a high voltage of 300kV. The point resolution of the microscope is 2Å and the information limit is 1.4Å. An Oxford instruments Link energy dispersive X-ray spectrometer is installed with which the local composition of the specimen can be determined.

Results

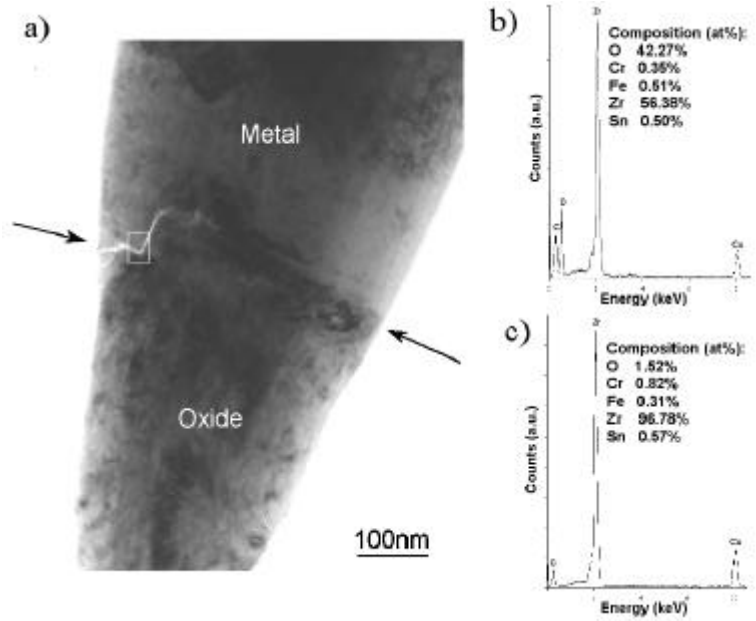

Figure 2. a) TEM image of the interface between the metal and the oxide layer. The black arrows indicate the location of the interface. b) EDX-spectrum recorded with the beam focused on the area below the interface and c) with the beam focused on the area above the interface.

A TEM image of the metal-oxide interface is shown in figure 2a. The dark line between the two black arrows marks the transition from one phase to another one, but it can not be determined directly which interface is shown here. Therefore the composition of the sample above and below the line of contrast is determined with EDX. The spectrum in figure 2b was recorded with the electron beam focused on the region below the interface. Apart from a high Zr signal, also a significant oxygen signal is recorded. The Cu and C signals are generated respectively by the specimen holder and by contamination and must be ignored for determining the composition of the specimen. Although the quantitative analysis does not exactly agree, it can be concluded that this region belongs to the oxide layer. The spectrum in figure 2c, on the other hand, shows the EDX-spectrum recorded with the electron beam focused on the region above the interface. It still contains a large Zr-peak, but the oxygen signal has completely disappeared. This indicates that this region belongs to the metal and that the dark line marks the interface between the metal and the oxide layer.

The exact grain structure in the oxide layer can not be deduced from this image. No contrast is observed that can be related to the boundary between two grains. Also no cracks or pores are observed. This means that a dense oxide layer is formed. Only at the interface between the metal and the oxide a small area has become amorphous. At the interface large stresses occur because of the lattice mismatch between the metal and the oxide. These stresses are accommodated for by the entire oxide phase. However, during specimen preparation a large amount of material is removed. As a result the large stresses can no longer be accommodated for and the oxide layer will relax and become partially amorphous.

Phase	Structure	Lattice parameters	Angles
Zr	Hexagonal	a = b = 3.232 Å c = 5.147 Å	$\alpha = \beta = 90°$ $\gamma = 120°$
ZrO_2	Tetragonal	a = b = 3.5917 Å c = 5.179 Å	$\alpha = \beta = \chi = 90°$
	Monoclinic	a = 5.145 Å b = 5.212 Å c = 5.312 Å	$\alpha = \gamma = 90°$ $\beta = 99.227°$

Table 1. Lattice parameters of Zircaloy-4, tetragonal zirconium oxide and monoclinic zirconium oxide.

The interface between the metal and the oxide layer was investigated in high resolution TEM (HRTEM). The crystallographic structure and lattice parameters of Zircaloy-4, tetragonal zirconium oxide and monoclinic zirconium oxide are given in table 1. Using these parameters all interplanar distances and angles can be calculated and compared with the values measured in the HRTEM images.

The area shown in figure 3a corresponds with the area in the white rectangle of figure 2a. The bottom part of the image should correspond with the oxide layer. The largest interplanar distances are measured to be 3.6 Å and 3.6 Å and the angle between these two planes is 90°. These values correspond exactly with the a- and b-lattice parameter of tetragonal zirconium oxide. This indicates that here a tetragonal oxide grain is present that is oriented along the [001] zone. Figure 3c shows the projection of a few unit cells of tetragonal oxide on the (001) plane. The

location of the zirconium atoms corresponds with the location of the white dots, while the oxygen atoms do not scatter the electrons significantly and are not visible in this image.

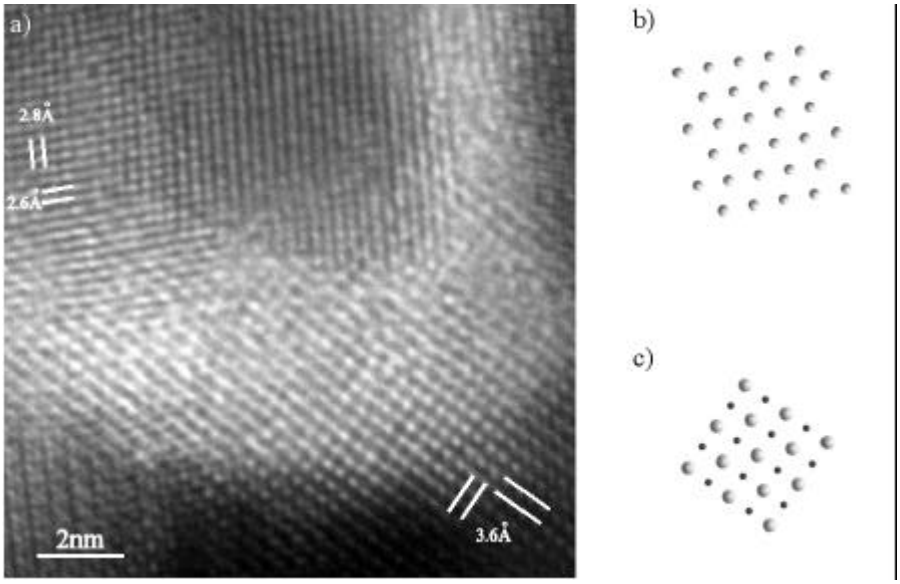

Figure 3. a) High resolution TEM image of the area within the white rectangle of figure 2a. b) Projected structure of Zircaloy-4 on the $(11\bar{2}0)$ *plane. c) Projected structure of tetragonal zirconium oxide on the (001) plane. The larger circles represent the zirconium atoms, while the smaller circles represent the oxygen atoms.*

For confirmation, the interplanar distances in the upper part are measured. The distances are 2.8 Å and 2.6 Å and the interplanar angle equals 87°. These values correspond well with the values expected for pure Zircaloy-4 oriented along the $[11\bar{2}0]$ zone. The projection of the structure of Zircaloy-4 on the $(11\bar{2}0)$ plane is shown in figure 3b and indeed corresponds very well with the observed image.

More information about the epitaxy between the metal and the oxide layer can be deduced from figure 3a. The (0001) basal planes of Zircaloy-4 lie parallel to the interface, while in the oxide layer, the (110) plane is parallel with the interface. From these observations the epitaxial relation between the metal and the oxide can be determined to be:

$$[001](110)_t \,//\, [11\bar{2}0](0001)_{Zry}$$

In which the subscript *t* stands for the tetragonal oxide phase and the subscript *Zry* for the Zircaloy-4 phase.

Further away from the interface also the monoclinic oxide phase starts to occur. The high resolution image of figure 4a can only correspond with the monoclinic structure. The interplanar distances are 2.5 Å and 2.6 Å and the angle between these planes is 99°. These measurements correspond with the values of the monoclinic oxide phase oriented on the [010] zone. The projection of the structure of monoclinic oxide on the (010) plane is shown in figure 4b. There is again a good agreement between the image and the schematic representation when it is considered that the oxygen atoms do not introduce contrast in the image.

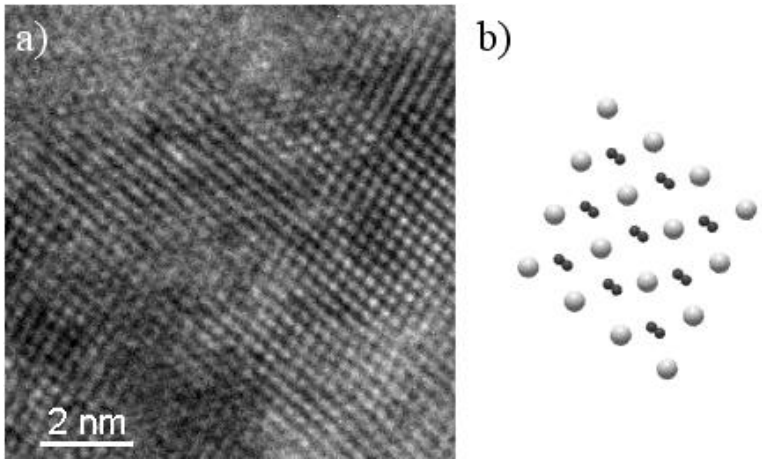

Figure 4. a) HRTEM image of a monoclinic oxide grain oriented along the [010] zone. b) Monoclinic oxide structure projected on the (010) plane. The large circles correspond with the zirconium atoms and the small circles correspond with the oxygen atoms.

Discussion

This investigation shows that TEM can be applied for the investigation of the microstructure of materials and to investigate interfaces between two different phases. At low resolution the location of the interface between two grains was located and using EDX the chemical composition of these grains was determined. High resolution images give information about the orientation of the grains and the organization of the atoms at the interface.

As already mentioned in the introduction, the interpretation of HRTEM images is not always straightforward. The image only shows the projection of the crystal structure on a particular plane. Therefore only columns of atoms are visualized, while individual atoms can not be detected. If the crystal is not perfectly oriented, the measured interplanar distances will deviate from the real distances. A second problem is that not all atom columns are visible in the image. Lighter atoms do not scatter the electrons as much as heavier atoms and will usually not be visible in the HRTEM images. For example, the oxygen atoms were not observed. Even differences in height between two columns can make some columns extinct. For example, in figure 3a the zirconium atom columns in the centre of the unit cell of the tetragonal oxide are barely or at some locations even not visible. For a correct interpretation image simulations must be performed.

The reported results are in very good agreement with the results already reported in literature [12]. It was shown that a dense oxide layer without cracks or pores is formed in the pre-transition region. Moreover, the high resolution images show that the first oxide phase on top of the metal is indeed the tetragonal oxide phase. Further away from the interface, also the monoclinic oxide phase was found.

According to literature, the tetragonal phase can be stabilized by a combination of three factors. First, the large volume of the oxide introduces large compressive stresses in the oxide layer [13]. Next, the second phase particles are reported to have a stabilizing effect on the tetragonal phase. These precipitates are more noble that the zirconium and will remain unoxidised in the oxide layer close to the interface. There they will start to oxidize and deplete in iron, which causes the stabilizing effect [14]. Finally, there is the small grain size effect [15]. The tetragonal phase has a lower surface energy than the monoclinic phase. In small grains, having a larger

surface to volume ratio, the difference in surface energy compensates the increase of internal energy and stabilizes the tetragonal phase.

The presence of large stresses near the metal-oxide interfaces is probably responsible for the amorphization of the area around the interface as observed in figure 3a. In the cladding before the specimen preparation a large number of atoms are present that accommodate for these high stresses. During specimen preparation, a large amount of material is removed. Locally insufficient atoms will be present to accommodate the stress and this can result in a reorganization of the atoms and possibly in a local amorphization at the interface.

The orientation of the metal and oxide is in agreement with the texture of the Zircaloy-4 cladding [16]. During the production process the grains are oriented such that the basal planes make an angle of preferentially 35° with the radial direction of the cladding. This means that the basal planes will lie almost parallel with the interface, as can be seen in figure 3a.

Conclusions

High resolution transmission electron microscopy in combination with energy dispersive X-ray spectroscopy was successfully applied for the investigation of the grain structure of the oxide layer formed during autoclave corrosion experiments and the investigation of the interface between the metal and the oxide.

The results for a specimen that was corroded in steam for 1 day are in good agreement with literature. On top of the metal a tetragonal zirconium oxide phase is formed that acts as a barrier layer against the further oxidation of the metal. Above the tetragonal layer also monoclinic oxide grains have been observed. No cracks or pores are present in the oxide layer, which confirms the fact that a dense oxide is formed when corroding the Zircaloy-4 cladding in steam.

References

1. Cheng B.C., Kruger R.M. and Adamson R.B., in *Zirconium in the Nuclear Industry: Tenth International symposium, ASTM STP 1245*, pp. 400-418 (1994).

2. Adamson R.B., in *Zirconium in the Nuclear Industry: Third International Symposium, ASTM STP 633*, pp. 326-343 (1977).

3. Adamson R.B., in *Zirconium in the Nuclear Industry: Twelfth International Symposium, ASTM STP 1354*, pp. 15-31 (2000).

4. Holt R.A. and Gilbert R.W., *J. Nucl. Mater.* **137,** p. 185 (1986).

5. Griffiths M. and Gilbert R.W., *J. Nucl. Mater.* **150**, p. 169 (1987).

6. Motta A.T., *J. Nucl. Mater.* **244**, p. 227 (1997).

7. Lefebvre F. and Lemaignan C., *J. Nucl. Mater*. **248**, p. 268 (1997).

8. Amelinckx S., Van Dyck D., Van Landuyt J. and Van Tendeloo G., *Handbook of Microscopy: Applications in Materials Science, Solid-State Physics and Chemistry* (VCH, Weinheim, 1997).

9. Williams D.B. and Carter C.B., *Transmission Electron Microscopy*, (Plenum Press, New York, 1996).

10. Spence J.H., *Experimental High-Resolution Electron Microscopy*, (Clarendon Press, Oxford, 1981).

11. Hillner E., *Zirconium in the Nuclear Industry: Third International Symposium, ASTM STP 633*, pp. 211-235 (1977).

12. Anada H. and Takeda K., *Zirconium in the Nuclear Industry: Eleventh International Symposium, ASTM STP 1295*, pp. 35-54 (1996).

13. Godlewski J., in *Zirconium in the Nuclear Industry: Tenth International Symposium, ASTM STP 1245*, pp. 663-686 (1994).

14. Pêcheur D., Lefebvre F., Motta A.T., Lemaingnan C. and Wadier J.F., *J. Nucl. Mater.* **198**, p. 318 (1992).

15. Garvie R.C., *Journal of Physical Chemistry* **69**, p. 1238 (1965).

16. Charquet D., Alheritière E. and Blanc G., *Zirconium in the Nuclear Industry, Seventh International Symposium, ASTM STP 939*, pp. 663-672 (1987).